Numerical Methods in Civil Engineering, 9-1 (2024) 01-15

Numerical Methods in Civil Engineering

Journal Homepage: https://nmce.kntu.ac.ir/

Quantifying the Extent of Damage in a Moment-resisting Frame Caused by Ground Motions using Normalized Discrete Wavelet Coefficients

Seyyed Meisam Aghajanzadeh*, Mohammadreza Mashayekhi**

ARTICLE INFO

RESEARCH PAPER

Article history:
Received:
April 2024
Revised:
June 2024
Accepted:
July 2024

Keywords:
Normalized Discrete Wavelet Transform;
Extent of Damage;
Moment Resisting Frame;
Signal Processing

Abstract:

This study presents a novel method to quantify the damage gradually developed during an earthquake. A damage-sensitive parameter is introduced based on the normalized wavelet decomposition of representative vibration signals during an earthquake. Story acceleration and roof displacement are representative vibration signals. Furthermore, the study examines the effects of the number of floors, PGA, PGA/PGV, and Impulsivity Index on the robustness of the proposed method. Four seismic ground motions are applied to the 6 and 8-story moment resisting frames. The results of the analyses show that the proposed method quantifies the extent of the damage using story acceleration. However, a damage-sensitive parameter based on roof displacement cannot accurately quantify the damage. The suggested damage-sensitive parameter depends more on earthquake properties than on structure characteristics. Among PGA, PGA/PGV, and Impulsivity Index, the damage-sensitive parameter is related to the Impulsivity Index of the ground motions.

1. Introduction

From numerous old infrastructures and ancient buildings to multiple modern structures, all of these are vulnerable to the negative effects of short-term, and long-term damages caused by human-induced activity and environmental factors such as corrosion, fatigue, material properties' degradation, earthquake, and fire-induced damage. These issues can age and shorten the structure's life cycle [1-3]. Among different experimental and computational techniques for damage detection [4, 5], vibration-based methods are a promising technique [6]. Damages in structures change dynamic characteristics which leads to changes in the structural vibration characteristics, allowing practical detection of potential damage by vibration-based techniques [7, 8].

Within vibration-based methods, which encompass modal approaches and signal processing techniques, the wavelet transform method has become widely used [9-12]. These methods include extracting features and analyzing the structural vibration responses to effectively detect potential damage in buildings or other structures [13, 14].

Newland is one of the pioneers of utilizing wavelet transforms for signal processing, even though his work does not specifically address the issue of damage detection [15, 16]. An application of wavelet theory in damage detection was considered by Surace and Ruotolo [17]. They identified the presence of the crack in the simulated response of a simple cantilever beam employing wavelet transform. The cantilever beam was simulated by finite element method and a dynamic force was applied [17]. Liew and Wang detect a transverse on-edge non-propagating open crack in a simply supported beam by the wavelet theory [18]. Wang and Deng utilized the wavelet transform to identify a transverse crack in a beam and a through-thickness crack in a plate [19]. Bayiss et al. detected and localized damage in a concrete plate model and a steel plate girder of a bridge using wavelet analysis. They decomposed the vibration response into discrete energy distributions as a floor function of time and scale using the continuous wavelet transform [20]. In an experimental study, Patel et al. suggested a wavelet-based

* *Assistant Professor, Department of Civil Engineering, University of Mazandaran, Babolsar, Iran. E-mail: s.m.aghajanzadeh@umz.ac.ir*
** *Corresponding author: Assistant Professor, Department of Civil Engineering, K. N. Toosi University of Technology, Tehran, Iran. E-mail: m.mashayekhi@kntu.ac.ir*

https://doi.org/10.52547/NMCE.2404.1050

method employing complex continuous Gaussian wavelet transformation for damage detection in a 6-story 1/3 scaled reinforced concrete structure [21]. Jahangir et al. determined the locations and extent of damages in RC beam specimens using an entropy-based wavelet transform [22]. Fallahian et al. detected damage by a combination of ensemble pattern recognition models and wavelet analysis techniques. They considered stiffness reduction as the damage indicator and five damage scenarios were introduced [23]. Thoriya et al. monitored and quantified mass loss because of corrosion of rebar embedded in concrete members by wavelet transform of conductance signature of the electromechanical impedance technique [24]. Beheshti-Aval et al. investigated the robustness of the wavelet transform method to detect small damage in a plate subjected to a harmonic loading with specified frequency and location. They showed that local perturbations of damages can be detected with the desired resolution by sudden changes in the spatial variation of the transformed response. They concluded that the use of the harmonic response is more efficient than the static response [25].

Among the various environmental hazards that pose a threat to structural safety, one of the main concerns is earthquakes, which can reduce the lifetime of buildings [26, 27]. In recent decades, wavelet analysis has been also used to detect structural damage caused by strong ground motion [28]. Goggins et al. utilized a wavelet-based equivalent linearization technique to evaluate stiffness degradation because of the yielding and buckling of braced members in a single-story concentrically braced frame subjected to scaled El Centro ground motions [29]. Todorovska and Trifunac investigated the former Imperial Country Services Building using a basis of bi-orthogonal wavelets based on detecting abrupt changes in the recorded seismic responses [30]. Vafaei and Adnan investigated the damage induced by strong ground motions to the tall airport traffic control towers of Kuala Lumpur International Airport. First, they identified the damaged locations through nonlinear time history analyses. Furthermore, the acceleration responses of these damaged regions are studied using continuous wavelet transform (CWT) and discrete wavelet transform (DWT). In their study, CWT only detects damaged elements reaching the ultimate curvature value, while DWT detects damage equivalent to the yielding value [31]. Aguirre et al. detected the rebar fracture by fast wavelet transform (FWT) and the frequency shift by continuous wavelet transform (CWT) for a reinforced concrete bridge column subjected to seismic excitation [32]. Quiñones et al. detect damage in a numerical model of a five-story shear building under seismic accelerations utilizing wavelet-based methodologies. The damage was introduced to the numerical model by suddenly reducing the stiffness of the first floor [33]. Pnevmatikos et al. suggested that a spike region indicates the development of plastic regions in a structure. This is based on wavelet transforms derived from the floor story acceleration induced by earthquake excitation [34]. He et al. proposed the time-varying frequency extraction method based on wavelet packet decomposition for assessing multi-dimensional seismic damage. They accurately capture the evolution and ultimate degree of damage. They suggested a time-varying synthetic damage index based on the reduction of the equivalent stiffness [35].

Although there are numerous studies on damage detection in structures, many limitations exist regarding methods for assessing the extent of seismic damage. These methods have limitations in that simulated damages must involve a sudden change in the dynamic properties of a structure [17, 30] or a preliminary analysis is essential to detect the location of the damage [29, 31]. On the other hand, some studies assess the extent of the damage based on modal-based methods including frequency and stiffness analysis. These methods can be challenging to calculate or obtain accurate material properties [35, 37, 38].

This study introduces a method that uses performance levels as defined in FEMA 273 [36] for quantifying the extent of the damage in structures immediately after strong ground motions; rather than just detecting the occurrence of the damage. FEMA 273 classifies structural performance levels as Immediate Occupancy Performance Level, Life Safety Performance Level, and Collapse Prevention Performance Level [36]. The method quantifies the damage in structures during an earthquake as a progressive process that develops in different parts of the structure based on damage-sensitive parameters suggested by Aghajanzadeh and Mashayekhi [39]. A straightforward explanation was put forth by Aghajanzadeh and Mashayekhi to detect structural damages as structural elements gradually shift towards plastic regions. However, they did not address the relationship between the structure's damage intensity and their proposed damage-sensitive parameter [39]. This study presents an innovative technique for quantifying damage levels in moment-resisting frame. It calculates a damage-sensitive parameter using normalized discrete wavelet coefficients [39]. The quantified damage is associated with performance levels. The proposed damage-sensitive wavelet-based parameter quantifies the seismic damage under four distinct earthquakes. Also, the effects of the structure height and type of representative vibration signals are studied and the dependency of the proposed method on earthquake characteristics is investigated.

2. Damage Detection Methodology based on Wavelet Analysis

This study considers a Damage-Sensitive Parameter (DSP) calculated based on wavelet analysis of representative

vibration signals [39]. Wavelet analysis is a powerful mathematical technique that decomposes signals by some wavelet functions to characterize signal local features. The wavelet functions are defined by two parameters: scale, which is related to frequency, and translation, which is related to time [40]:

$$\psi_{a,b}(t) = \frac{1}{\sqrt{a}}\psi\left(\frac{t-b}{a}\right) \quad (1)$$

where a and b denote the scale and translation parameters. This allows for a more localized representation of signals, which can be particularly useful for analyzing signals with non-stationary or transient characteristics [4, 39]. The wavelet analysis of a signal f(t) gives its correlation with wavelets $\psi_{a,b}(a,b)$. The continuous wavelet transform (CWT) involves summing over all time f(t) multiplied by a scaled and shifted version of a mother wavelet as follows:

$$CWT(a,b) = \frac{1}{\sqrt{a}}\int_{-\infty}^{\infty} f(t)\psi\left(\frac{t-b}{a}\right)dt \quad (2)$$

Continuous wavelet analysis considers a continuous representation of signals in a wide range of mother wavelet coefficients spanning diverse scales. This issue is not computationally effective and requires considerable calculation efforts to find mother wavelet coefficients. To address this challenge, the Discrete Wavelet Transform (DWT) utilizes a constrained collection of dyadic scales and translations. In dyadic scales and translations, the dilatation parameter is defined as $a=2^j$ and the translation parameter is defined as $b=2^jk$, where (j,k) are integer numbers. The signal f(t) can be reconstructed by its approximation and details based on DWT as follows [31]:

$$f(t) = A_J + \sum_{j\leq J} D_j \quad (3)$$

where D_j is the detail at level j and it is calculated as

$$D_j = \sum_{k\in Z} a_{j,k}\psi_{j,k}(t) \quad (4)$$

where $\psi_{j,k}(t)$ is the mother wavelet function and it is defined as:

$$\psi_{j,k}(t) = 2^{\frac{j}{2}}\psi(2^j t - k) \quad (5)$$

and the approximation at level J is defined as:

$$A_J = \sum_{j>J} D_j \quad (6)$$

After calculating the details of the wavelet transform of a representative vibration signal for the healthy structure and its response during an earthquake, these two sets of wavelet transform details are normalized to reach a maximum value of 1. Finally, the damage-sensitive parameter (DSP) is defined as the area under the curve of the summation of differences between Wavelet Normal Decomposition of the structure's response during an earthquake and undamaged structure for the total of wavelet transform levels as [36]:

$$DSP(t_{tot}) = \int_0^{t_{tot}} \sum_{j=1}^{I}\left(D_{j-n}^{Recorded\ acceleration} - D_{j-n}^{Undamaged}\right)dt \quad (7)$$

where t_{tot} is the total duration of the recorded acceleration and 'I' corresponds to the complete count of wavelet transform levels, and for this study, it is 9. Furthermore, "n" denotes the normalization of wavelet decomposition coefficients.

3. Numerical Modeling

The suggested method for assessment of the seismic damage is applied to the 6-story and 8-story moment resisting frame. Figure 1 shows the moment resisting frame properties. MATLAB software computes details of wavelet transform based on fourth-order Daubechies basis function. ETABS software calculates the nonlinear dynamic response with a damping value of 3%. Dead and live loads are 3060 kg/m and 1200 kg/m, respectively. Beam sections are shown with the abbreviation PG, representing plate girders. The terminology is structured as PG-A×B×C, where A represents the web's height, B indicates the flange's width, and C represents the flange's thickness. The naming convention for column sections is BOX-A×B×C, where A represents the width, B represents the height, and C indicates both the flange and web thickness (Table 1).

Table 1: Cross-sectional profiles of beams and columns

story number	beam section		column section
	middle span	side span	
1	PG-30×20×1.2	PG-40×20×1.5	BOX-30×30×1.5
2	PG-30×20×1.2	PG-40×20×1.5	BOX-30×30×1.5
3	PG-30×20×1.2	PG-40×20×1.5	BOX-30×30×1.5
4	PG-30×20×1.2	PG-40×20×1.5	BOX-30×30×1.5
5	PG-30×20×1.2	PG-30×20×1.5	BOX-30×30×1.5
6	PG-30×20×1.2	PG-30×20×1.2	BOX-25×25×1.2
7	PG-30×20×1.2	PG-30×20×1.2	BOX-25×25×1.2
8	PG-30×20×1.2	PG-30×20×1.2	BOX-25×25×1.2

3.1 Damage Simulation in Structural Model

These plastic hinges are defined to the structures and their performance levels are studied based on procedures described in FEMA 273. Plastic hinges are deformation controlled. Figure 2 shows the moment-rotation curve for a hinge according to the FEMA 273 [36].

Points between A and B show a linear region of structural elements in which no damage has occurred. Point B where $\theta = \theta_y$ is the rotation at the yielding. After point B, there are plastic permanent rotation in the hinges. The region between points B and C shows the plastic behavior of structural elements.

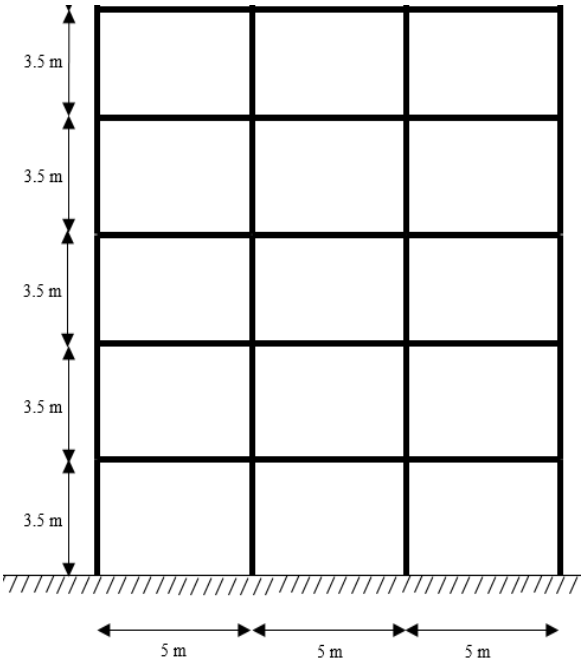

(a) 6-story frame

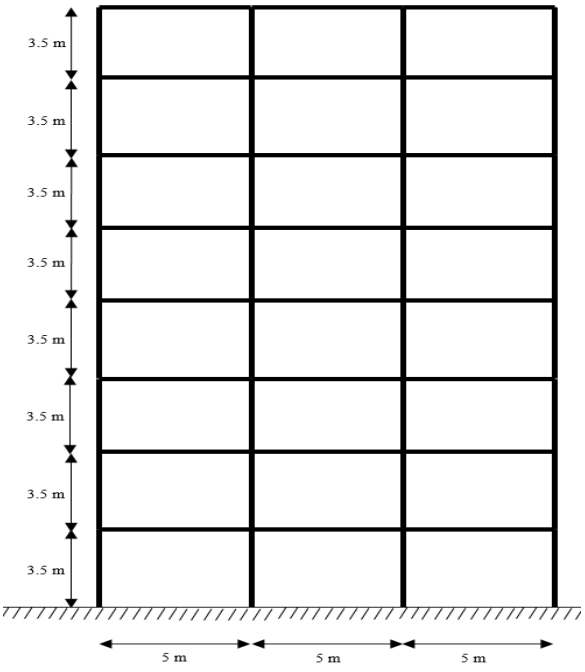

(b) 8-story frame

Fig. 1: Structural configuration under consideration

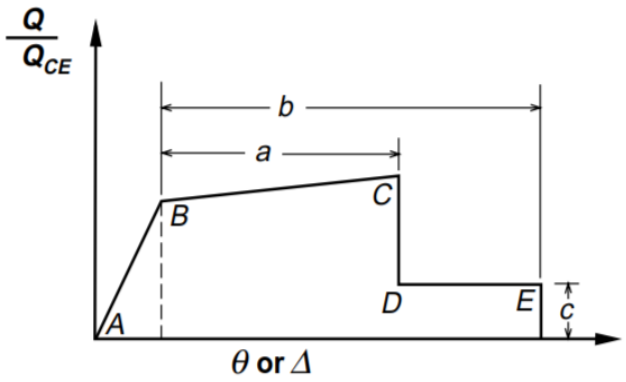

(a)

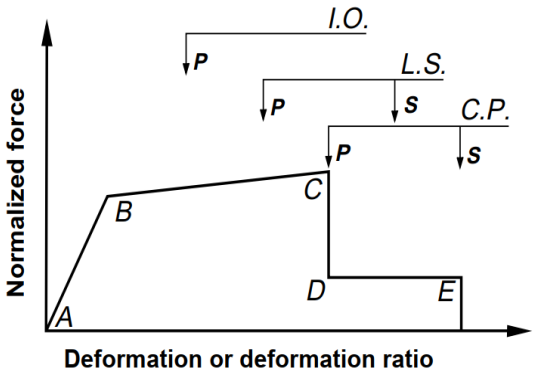

(b)

Fig. 2: (a) Moment-rotation curve (b) performance level [36]

At the plastic region, the response of the beam or column is calculated as a function of its rotation using the moment rotation. For beams and columns, θ_y, is calculated by Equations 8 and 9, respectively.

$$\theta_y = \frac{ZF_{ye}l_b}{6EI_b} \quad (8)$$

$$\theta_y = \frac{ZF_{ye}l_c}{6EI_c}(1 - \frac{P}{P_{ye}}) \quad (9)$$

For beams and columns, M_y is calculated by Equations 10 and 11, respectively.

$$M_y = ZF_{ye} \quad (10)$$

$$M_y = 1.18ZF_{ye}(1 - \frac{P}{P_{ye}}) \leq ZF_{ye} \quad (11)$$

The Strain-hardening slope is 3% of the elastic slope (slope between points B and C) and points C, D, and E are defined based on Table 5-4 in FEMA 273 [36].

For each structural analysis, based on the hinge status with maximum curvature, the extent of the damage for the moment-resisting frame is assigned. 17 different damage levels are considered for each seismic excitation to cover all regions of responses from linear to the point after C. Table 2 shows damage levels with their corresponding earthquake scale factor and damage level:

- Damage levels 1 to 4: 4 analyzes in the elastic region at line AB at the moment-rotation curve and

performance level Point A to Immediate Occupancy (IO),
- Damage level 5: 1 analysis corresponds to point B at the moment-rotation curve and performance level Point A to Immediate Occupancy (IO),
- Damage levels 6 to 9: 4 analyzes in the plastic region BC at the moment-rotation curve and performance level Immediate Occupancy (IO) to Collapse Prevention (CP)
- Damage level 10: 1 analysis associated with the initial point of Collapse Prevention (CP) performance level in the plastic region BC at the moment-rotation curve
- Damage levels 11 to 14: 4 analysis corresponds to the plastic region BC after Collapse Prevention (CP) performance level.
- Damage level 15: 1 analysis belongs to point C of the moment-rotation curve after Collapse Prevention (CP) performance level.
- Damage levels 16 and 17: 2 analyses for performance level after Collapse Prevention (CP) performance level after point C of the moment-rotation curve.

Table 2: Damage level for 8-story and 6-story frames according to PGA of each ground motion

Damage level	Moment rotation curve (Figure 2-a)	Performance level (Figure 2-b)	PGA (g)							
			Northridge Earthquake		Bam Earthquake		Kobe Earthquake		Manjil Earthquake	
			8-story	6-story	8-story	6-story	8-story	6-story	8-story	6-story
1	Line AB	Performance level Point A to Immediate Occupancy (IO)	0.12	0.12	0.10	0.10	0.07	0.07	0.16	0.16
2			0.14	0.18	0.12	0.12	0.12	0.12	0.21	0.26
3			0.16	0.24	0.14	0.13	0.16	0.16	0.26	0.36
4			0.18	0.31	0.17	0.15	0.19	0.19	0.31	0.47
5	Point B		0.20	0.35	0.21	0.16	0.22	0.22	0.34	0.58
6	Plastic region BC	Performance level Immediate Occupancy (IO) to Collapse Prevention (CP)	0.41	0.53	0.33	0.29	0.28	0.32	0.57	0.88
7			0.61	0.71	0.50	0.42	0.40	0.41	0.83	1.20
8			0.82	0.90	0.66	0.55	0.52	0.50	1.09	1.56
9			1.02	1.08	0.83	0.69	0.61	0.60	1.46	1.92
10	Plastic region BC	The initial point of Collapse Prevention (CP) performance level	1.22	1.26	0.99	0.83	0.70	0.68	1.66	2.29
11	Plastic region BC	After Collapse Prevention (CP) performance level	1.43	1.30	1.07	0.91	0.84	0.76	1.87	2.44
12			1.63	1.43	1.16	0.99	0.98	0.84	2.08	2.60
13			1.83	1.55	1.24	1.07	1.13	0.93	2.29	2.76
14			2.04	1.67	1.32	1.16	1.27	1.01	2.60	2.91
15	Point C	After Collapse Prevention (CP) performance level	2.24	1.75	1.40	1.24	1.41	1.08	2.86	3.07
16	After point C of the moment-rotation curve	After Collapse Prevention (CP) performance level	2.45	2.04	1.49	1.49	1.64	1.41	3.12	3.64
17			2.85	2.45	1.57	1.57	1.88	1.64	3.64	4.16

3.2 Ground motion records

Northridge, Bam, Kobe, and Manjil ground motion records are applied to the moment-resisting 6-story and 8-story frames (Figure 3 and Table 3). Different scale factors are considered for each ground motion to include the response of the structure from the state where all the elements are in the elastic region to the state where the responses in some elements have passed point C of the moment-rotation curve.

Table 3: Details of ground motion records

Earthquake	Station	Year	PGA
Northridge	Canyon Country - W Lost Cany	1994	0.40g
Bam	Bam	2003	0.81g
Kobe	Shin-Osaka	1995	0.23g
Manjil	Abbar	1990	0.51g

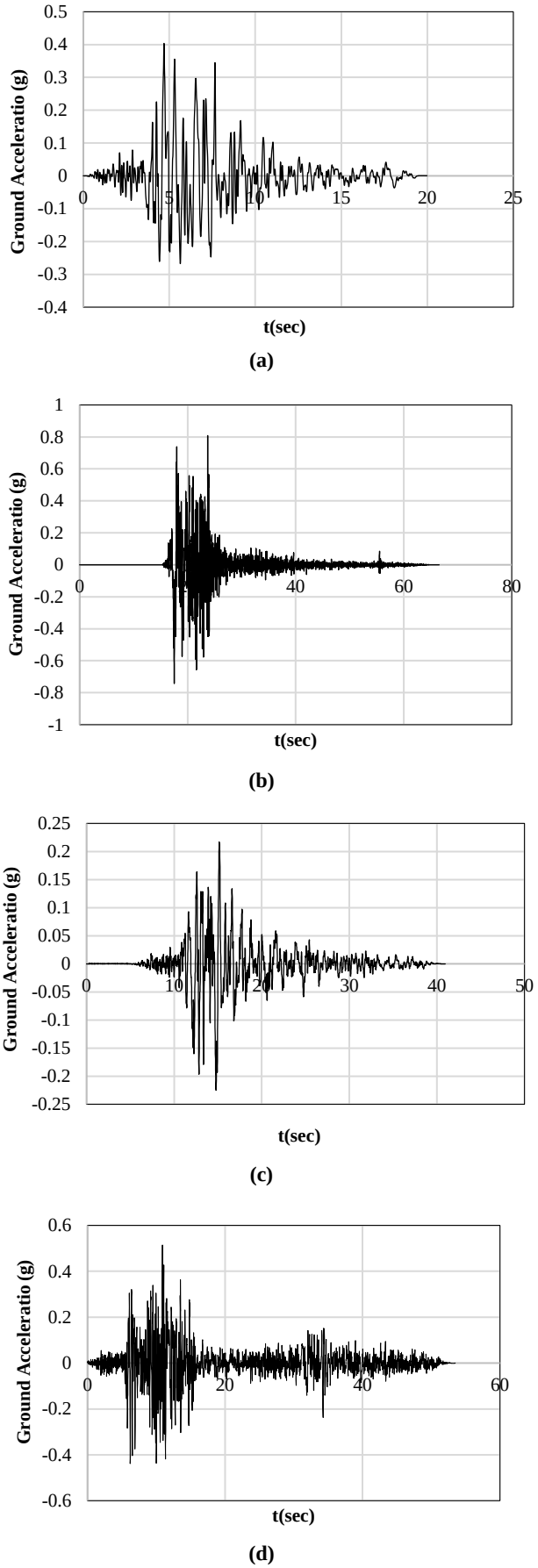

Fig. 3: (a) 1994 Northridge earthquake; (b) 2003 Bam earthquake, (c) 1995 Kobe earthquake; and (d) 1990 Manjil earthquake

4. Numerical Results

This study investigates the robustness of DSP(t_{tot}) to find information about the extent of the damage to the whole structure. Effects of different parameters including moment resisting frame height, type of representative vibration signal (Floor acceleration or roof displacement), and ground motion characteristics on the performance of DSP(t_{tot}) for damage assessment are studied.

4.1 Damage Sensitive Parameter based on Roof Displacement

Floor acceleration and displacement of the roof are parameters that is used to analyze the structure response. Figure 4 compares the damage levels based on two classes of DSP(t_{tot}): one based on floor acceleration and the other based on roof displacement.

DSP(t_{tot}) based on roof displacement shows higher values for all four earthquakes, especially in damage levels corresponding to the plastic region and regions after point C These two classes of structure response are more consistent for damage levels from 5 to 17 under earthquakes Northridge, Bam, Kobe, and Manjil. But, DSP(t_{tot}) based on roof displacement is approximately equal to 5 under Bam excitation for damage levels 1 to 5 (performance levels Point A to IO) which is not consistent with its corresponding values for Northridge, Kobe, and Manjil earthquakes.

DSP(t_{tot}) calculated based on floor acceleration at the 1st floor is equal to zero for damage levels 1 to 5. This inconsistency for performance levels Point A to IO leads to inefficiency of DSP(t_{tot}) calculated based on roof displacement for damage detection and also assessment of damage extent. Table 4 compares differences of DSP(t_{tot}) calculated based on floor acceleration and roof displacement for 3 damage levels 5, 10, and 15.

Table 4 shows that differences between DSP(t_{tot}) calculated based on roof displacement and floor acceleration increase from damage level 5 (point B) to damage level 10 (point CP), but are approximately constant from damage level 10 to damage level 15. This may show that by the development of plastic regions in structure, differences between these two classes of DSP(t_{tot}) gradually increase. Again, inconsistency of DSP(t_{tot}) based on roof displacement for Bam excitation is evident. Differences between these two classes of DSP(t_{tot}) for damage level 5 is equal to zero for 3 earthquakes Northridge, Kobe, and Manjil whereas this is 5.53 for bam earthquake. The robustness of DSP(t_{tot}) calculated based on roof displacement is questionable because of responses for Bam earthquake at damage levels 1 to 5 for performance levels Point A to IO.

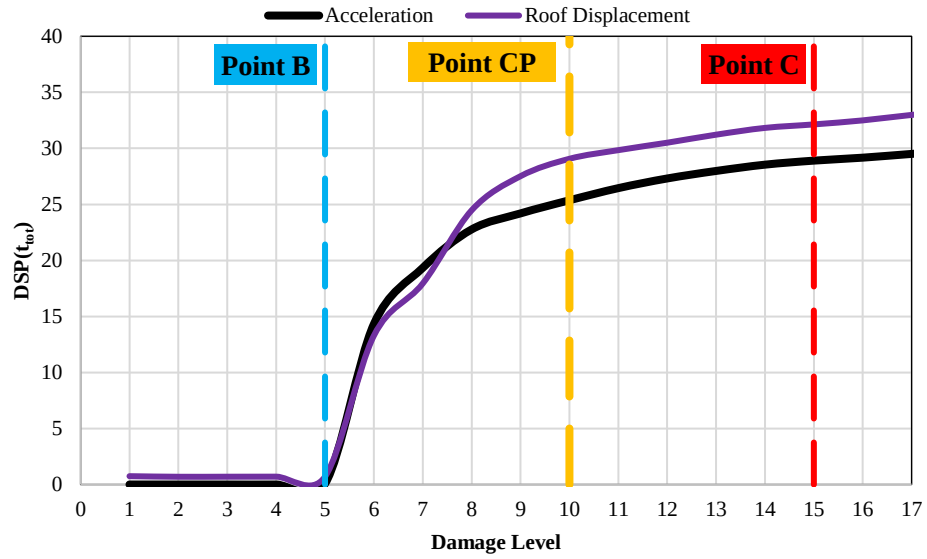

(4a) Northridge

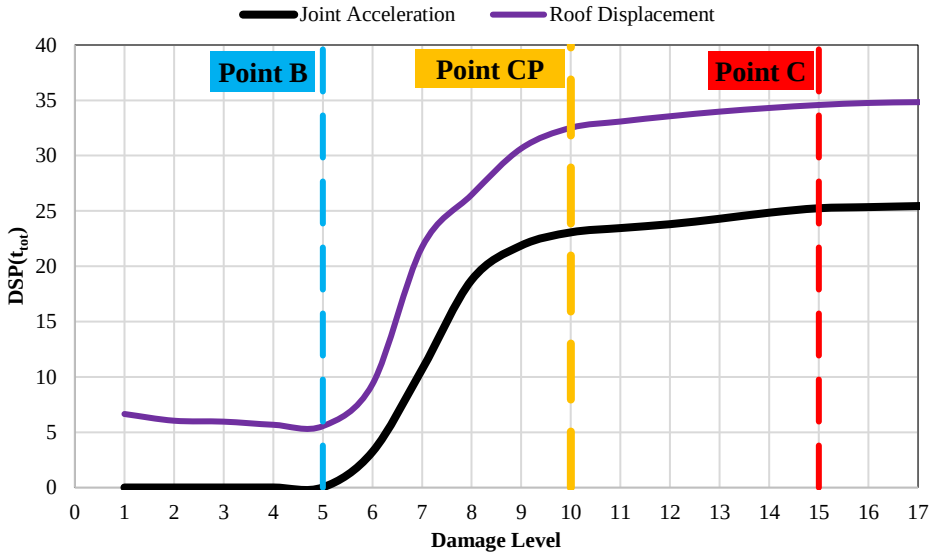

(4b) Bam

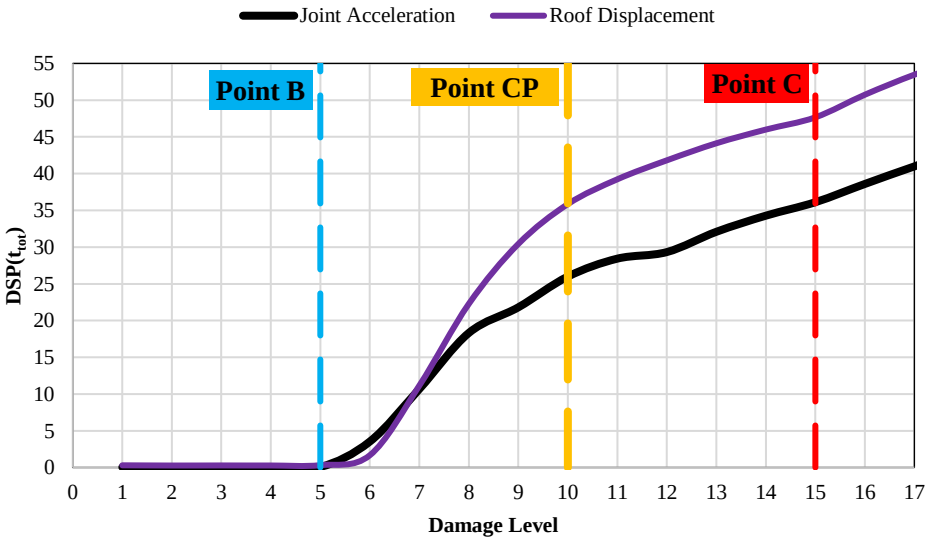

(4c) Kobe

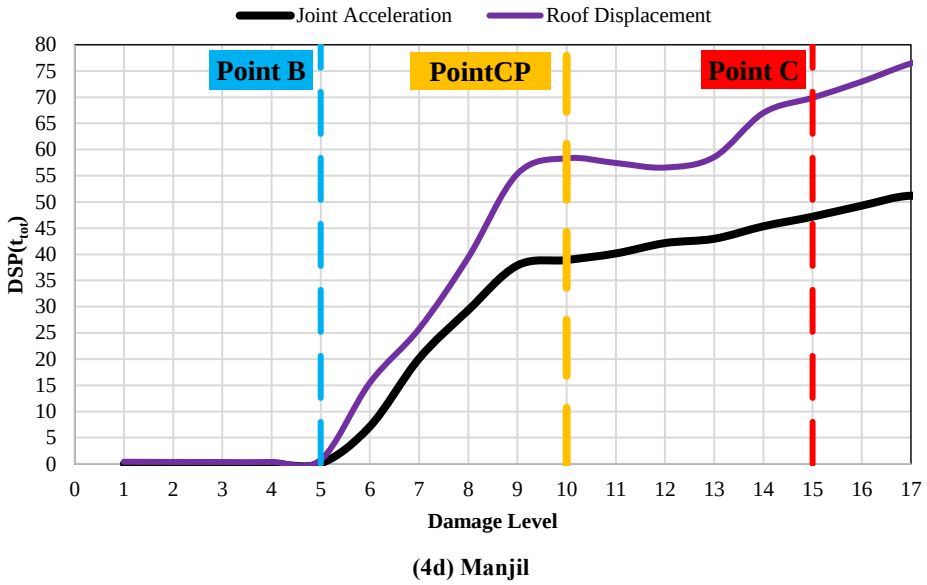

Fig. 4: Comparison between DSP(t_{tot}) calculated based on floor acceleration and roof displacement

Table 4: DSP(t_{tot}) based on floor accelerations and roof displacements for damage levels 5, 10, and 15

Earthquake	Vibration signals	DL 5 (Point B)	DL 10 (Point CP)	DL 15 (Point C)
Northridge	Roof displacement	0.71	29.07	32.14
	floor acceleration	0.07	25.37	28.90
	Differences	**0.64**	**3.70**	**3.24**
Bam	Roof displacement	5.55	32.52	34.58
	floor acceleration	0.02	23.07	25.25
	Differences	**5.53**	**9.45**	**9.33**
Kobe	Roof displacement	0.32	35.85	47.66
	floor acceleration	0.07	25.99	36.11
	Differences	**0.25**	**9.86**	**11.55**
Manjil	Roof displacement	0.78	58.34	69.89
	floor acceleration	0.07	38.92	47.19
	Differences	**0.71**	**19.42**	**22.7**

So, an explicit definition for damage detection and also extent of the damage is not possible based on DSP(t_{tot}) calculated by roof displacement whereas DSP(ttot) based on floor acceleration is more reliable for assessing the extent of the damage.

4.2 Damage Assessment based on Damage Sensitive Parameter

This section quantifies the damage based on damage sensitive parameter (DSP(t_{tot})) using defined damage levels 1 to 17 based on floor acceleration at the 1st, 4th, and 6th stories. Figure 5 shows that in all four earthquakes of Northridge, Bam, Kobe, and Manjil, the DSP(t_{tot}) of the first floor is higher. DSP(t_{tot}) shows similar trends for different stories that experience equal seismic ground motion. So, DSP(t_{tot}) is more influenced by the earthquake's characteristics rather than the floor number. But, when calculating DSP(t_{tot}), it's important to always consider a specific floor number. This study calculates DSP(t_{tot}) based on the story acceleration of the 1st story.

Figure 6 shows the damage assessed by the damage sensitive parameter (DSP(t_{tot})). DSP(t_{tot}) is sensitive to the damage level defined for the structures.

There are 3 specific regions in DSP(t_{tot}) based on damage level assigned to the structure: 1- region before the damage level 5 (point B) refers to the performance level of Immediate Occupancy (IO), 2- a region between damage levels 5 to 10 with excessive change in DSP(t_{tot}) corresponds to the performance level after Immediate occupancy (IO) and before collapse prevention (CP), 3- a region between damage levels 10 to 17 with slight variation for DSP(t_{tot}) after Collapse prevention (CP) performance level.

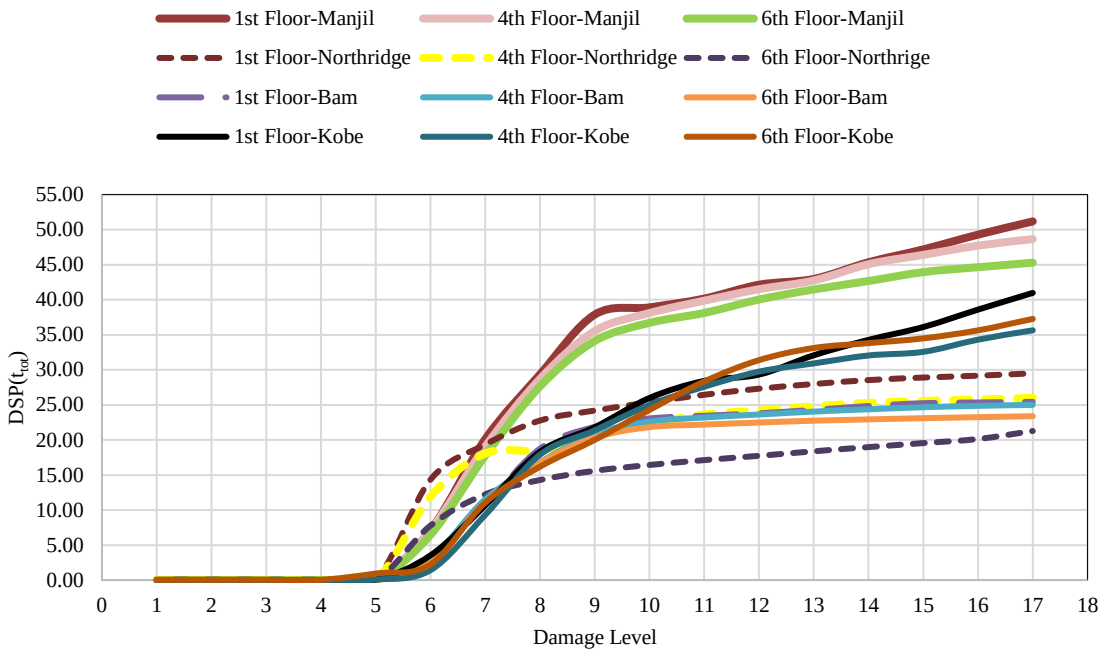

Fig. 5: Damage sensitive parameter (DSP(t_{tot})) for different stories subjected to the Northridge, Bam, and Kobe Earthquake

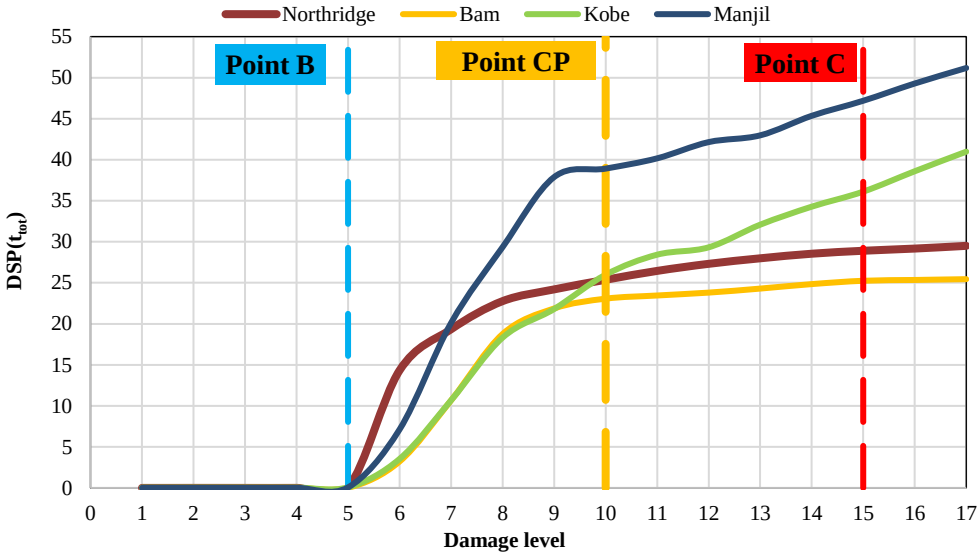

Fig. 6: Damage sensitive parameter (DSP(t_{tot})) for the 8-story frame subjected to the Northridge, Bam, Kobe and Manjil Earthquake

The range of DSP(t_{tot}) for damage levels 1 to 5 (performance levels Point A to IO) of the 8-story frame (linear responses) is almost zero, irrespective of the earthquake applied. DSP(t_{tot}) significantly increases as the 8-story frame moves from damage level 5 (linear region AB and performance levels Point A to IO) to damage levels 6 to 10 (plastic region BC at the moment-rotation curve and Performance level Immediate Occupancy (IO) to Collapse Prevention (CP)). Structural members are in the plastic region between damage levels 6 to 10, but their performance level does not exceed the collapse prevention point CP. The slope of DSP(t_{tot}) noticeably decreases after damage level 10 (point CP). But, an explicit structural damage assessment based on DSP(t_{tot}) is highly dependent on the earthquake characteristics. DSP(t_{tot}) at damage levels greater than 5 is different for each earthquake showing dependency of DSP(t_{tot}) to the earthquake characteristics. The illustration in Figure 6 indicates how DSP(ttot) tracks the evolution of the plastic region and their corresponding performance levels in an 8-story frame. But, DSP(t_{tot}) at damage levels 6 to 17 is different for each earthquake showing dependency of DSP(t_{tot}) to the earthquake characteristics.

Next, the effectiveness of DSP(t_{tot}) for damage assessment is compared with PGA efficiency. Figure 7 plots the damage level based on PGA of scaled earthquakes for the 8-story frame. Damage levels from 1 to 17 in terms of PGA show a

linear trend which is not consistent with the overall behavior of a moment-resisting frame discussed in studies [41]. But, damage level in terms of DSP(t_{tot}) shows three different regions. DSP(t_{tot}) of the first region is equal to zero, and for two other regions, there are linear relation between DSP(t_{tot}) and damage level. In these two regions, damages are developed in structures. Figure 6 and Figure 7 prove that damage level according to DSP(t_{tot}) is more consistent with the overall behavior of a moment-resisting frame characterized by structural performance levels than PGA.

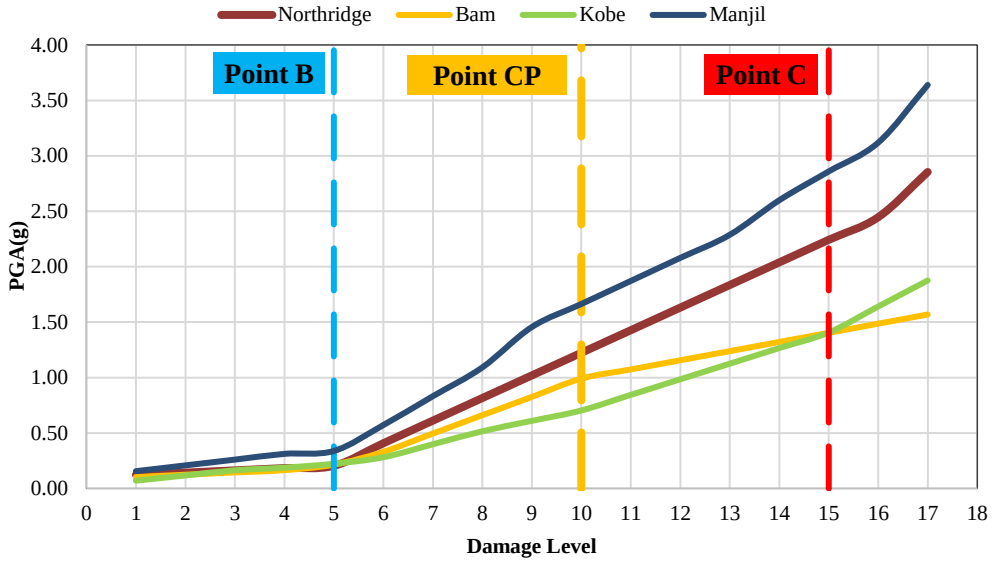

Fig. 7: Damage level based on PGA of scaled earthquakes for the 8-story frame

4.3 8-story versus 6-story Moment Resisting Frame

This section investigates the effects of moment resisting frame height on DSP(t_{tot}) for assessing the extent of the damage. Figure 8 shows the DSP(t_{tot}) of a 6-story frame, and compares it with the DSP(t_{tot})of the 8-story frame. In both structures, DSP(t_{tot}) is approximately equal to zero in the linear region. When DSP(t_{tot})≈0, regardless of the height of the structure, it indicates that all structural elements are within linear regions. The range of DSP(t_{tot}) demonstrates a notable increase after point B in damage levels ranging from 5 to 10, and the slope of its variation decreases after reaching damage level 10.

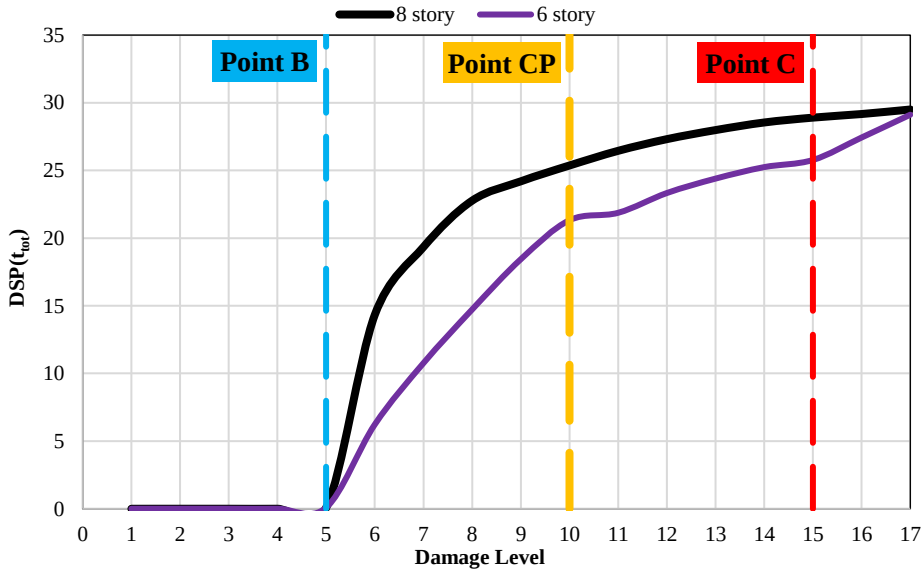

(8a) Northridge

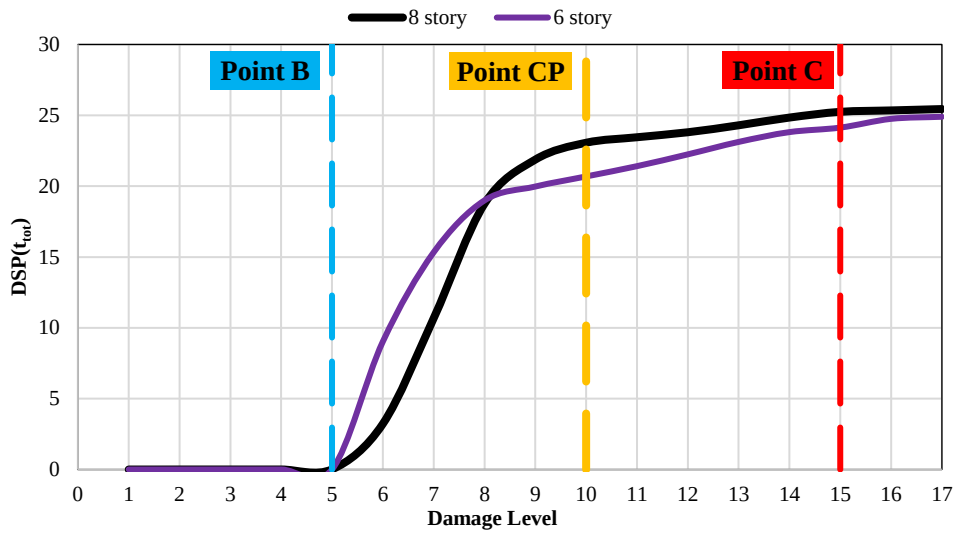

(8b) Bam

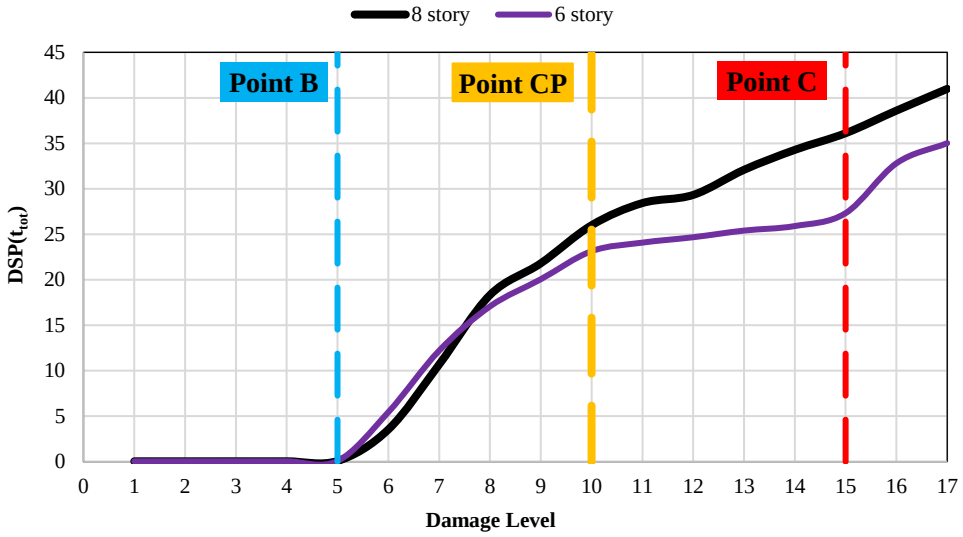

(8c) Kobe

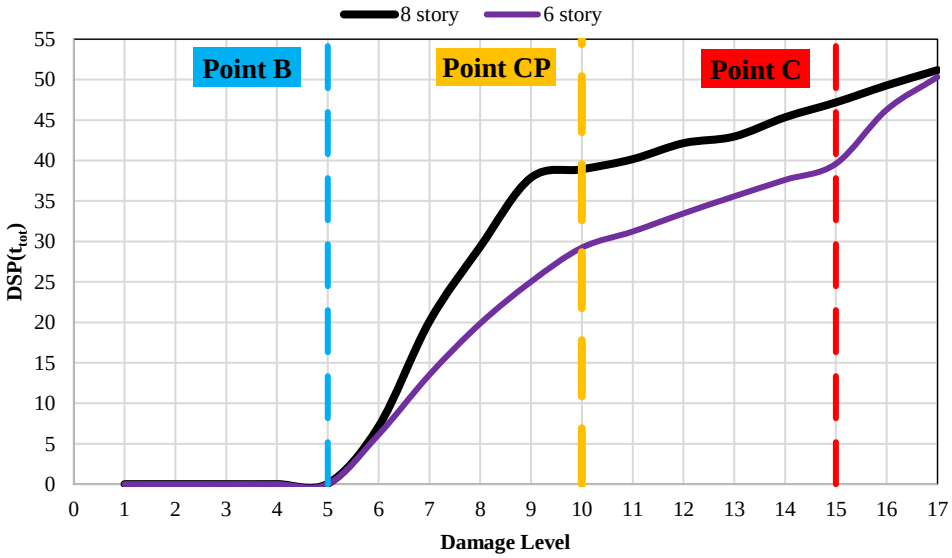

(8d) Manjil

Fig. 8: Comparison of DSP(t_{tot}) between 8-story and 6-story frames

Table 5: DSP(t_{tot}) for damage level

Earthquake	Structure	DL 5 (Point B)	DL 10 (Point CP)	DL 15 (Point C)
Northridge	6-story	0.09	21.33	25.77
	8-story	0.07	25.37	28.90
	Differences	**0.02**	**4.04**	**3.13**
Bam	6-story	0.01	20.69	24.13
	8-story	0.02	23.07	25.25
	Differences	**0.01**	**2.38**	**1.12**
Kobe	6-story	0.07	23.14	27.32
	8-story	0.07	25.99	36.11
	Differences	**0.00**	**2.85**	**8.79**
Manjil	6-story	0.01	29.24	39.60
	8-story	0.07	38.92	47.19
	Differences	**0.06**	**9.68**	**7.59**

For earthquakes, Northridge and Manjil, DSP(t_{tot}) of the 8-story frame is greater for damage levels 5 to 17. But, for earthquakes Bam and Kobe, the DSP(t_{tot}) of a 6-story frame is greater between damage levels 5 to 8 and again is less than the DSP(t_{tot}) 8-story between damage levels 8 to 17. Dependency of DSP(t_{tot}) to the earthquake characteristics for both 6-story and 8-story frames are evident. Table 5 shows differences in DSP(t_{tot}) for 6-story and 8-story frames including the Northridge, Bam, Kobe, and Manjil earthquakes.

4.4 Earthquake Characteristics

This section considers the effects of different earthquake characteristics on DSP(t_{tot}) for damage assessment in the moment-resisting frame. First, the dependency of DSP(t_{tot}) to PGA is studied. Figure 9 illustrates the effects of scaled records PGA on DSP(t_{tot}). For equal PGA, each record has a different DSP(t_{tot}) value, in which these differences are more evident for greater PGA. Damages are more developed for Records with higher PGA. So, the effects of PGA on DSP(t_{tot}) for estimating the damage extent is not a straightforward relationship.

Next, the effects of earthquake frequency contents on DSP(t_{tot}) are studied. Pavel and Lungu showed that the ratio PGA/PGV is a more satisfactory criterion for assessing the overall frequency content of seismic excitation [42]. This ratio classifies the ground motion frequency contents as low range with PGA/PGV<0.8, medium range with 0.8≤ PGA/PGV≤1.2, and high range with PGA/PGV>1.2.

Table 6 compares the ratio PGA/PGV of each ground motion including DSP(t_{tot}) of 8-story and 6-story frames for damage levels 5, 10, and 15.

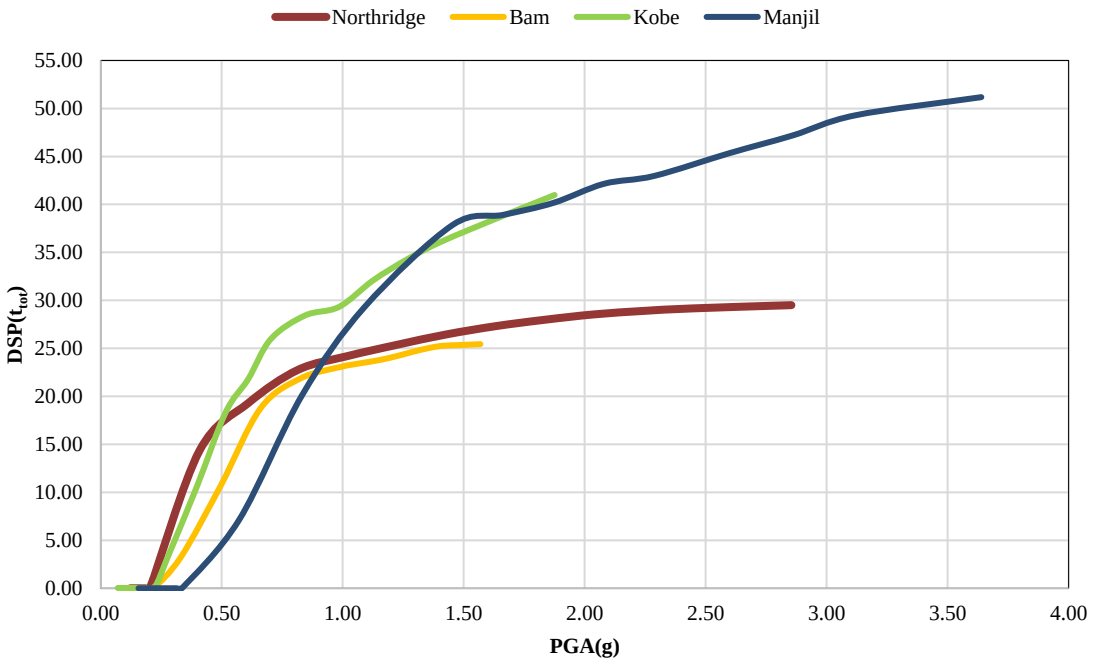

Fig. 9: Effects of scaled records PGA on DSP(t_{tot})

Manjil with a higher ratio and Bam with a lower ratio of PGA/PGV exhibits respectively higher and lower DSP(t_{tot}) at damage levels 10 and 15 of 8-story and 6-story frames. But ground motion Northridge has less DSP(t_{tot}) with a greater ratio of PGA/PGV compared to the Kobe earthquake. So, the effects of frequency content on DSP(t_{tot}) for assessing the extent of the damage in structure is arguable. This argument is valid for both 6-story and 8-story frames with different structural periods. So, the effects of earthquake parameters are more dominant than structural characteristics.

Table 6: Classification of earthquake frequency contents based on PGA/PGV

Earthquake	PGA (g)	PGV (cm/sec)	PGA/PGV	Classification	DSP(t_{tot}) of 8-story frame		DSP(t_{tot}) of 6-story frame	
					DL 10	DL 15	DL 10	DL 15
Bam	0.81	124.12	0.64	low	23.07	25.25	20.69	24.13
Kobe	0.23	31.33	0.72	low	25.99	36.11	23.14	27.32
Northridge	0.40	44.38	0.88	medium	25.37	28.90	31.33	25.77
Manjil	0.51	42.46	1.17	medium	38.92	47.19	29.24	39.60

Finally, different parameters of the Northridge, Bam, Kobe, and Manjil earthquakes are studied. Among these ground motion parameters, the Impulsivity Index (IP) [43] shows a meaningful relation with the sequence of DSP(t_{tot}) calculated for each of the 4 earthquakes. The Impulsivity Index (IP) is an indicator of the impulsive character considering the development length of velocity and PGV which is defined as follows:

$$IP = \frac{Ld_v}{PGV} \quad (12)$$

where PGV is the peak ground velocity and Ld_v is developed length of velocity which is defined as follows:

$$Ld_v = \sum_{i=1}^{n} \left(\sqrt{\Delta t^2 + \Delta v_i{}^2} \right) \quad (13)$$

where n is the number of discrete values of seismic ground motions, Δt is the time step of the recorded ground motion and Δv_i is the velocity increment between to time of t_i and t_{i+1}. For a more exact analysis, the DSP(t_{tot}) of scaled earthquakes with PGA=g is calculated. Table 7 shows the Impulsivity Index (IP) of ground motions and their corresponding DSP(t_{tot}). The effects of ground motions on DSP(t_{tot}) for assessing the extent of damage are associated with the Impulsivity Index (IP) of each earthquake. The earthquake with the highest Impulsivity Index (IP) has the highest DSP(t_{tot}) at damage levels 5 and 10 for both 6 and 8-story frames. So, one needs to consider DSP(t_{tot}) in conjunction with the Impulsivity Index (IP) to assess the extent of damage in a structure.

Table 7: Impulsivity Index (IP) of ground motions and their corresponding DSP(t_{tot})

Earthquake	PGA	Scale factor	Impulsivity Index (IP)	DSP(t_{tot}) of 8-story frame		DSP(t_{tot}) of 6-story frame	
				DL 10	DL 15	DL 10	DL 15
Bam	0.81g	1.24	17.87	23.07	25.25	20.69	24.13
Northridge	0.40g	2.5	20.44	25.37	28.90	31.33	25.77
Kobe	0.23g	4.48	23.13	25.99	36.11	23.14	27.32
Manjil	0.51g	1.96	49.11	38.92	47.19	29.24	39.60

5. Conclusion

This study quantifies the extent of damage in a structure using a damage-sensitive parameter called DSP(t_{tot}). Floor acceleration on 1st floor. 17 damage levels based on the status of the hinge with maximum curvature are considered, including four distinct ground motions. 6 and 8-story moment resisting frames are considered. DSP(t_{tot}) is calculated once using floor acceleration and the other is roof displacement. Different earthquake properties including PGA, PGA/PGV, and Impulsivity Index (IP) of ground motions are studied. The following results are outlined:

- This methodology only depends on structural response histories.
- DSP(t_{tot}) based on floor acceleration captures the extent of the damage. However, a general relationship between DSP(t_{tot}) and the extent of damage needs a more detailed investigation considering seismic characteristics and structure properties.
- It is not possible to explicitly define damage detection and assess the extent of the damage based on the DSP(t_{tot}) calculated by roof displacement.
- For the exact assessment of damage, a preliminary analysis is required to capture the DSP(t_{tot}) profile of a structure. If a profile for DSP(t_{tot}) corresponds to each earthquake is available, the amount of damage and its corresponding damage levels are easily detectable.
- Even without a profile and just one record from the structural response, the amount of damage in the structure is approximately detectable:
  - When DSP(t_{tot}) is greater than 5 and less than 20, it indicates that certain structural elements are in the plastic region. But their corresponding performance level is between Immediate Occupancy and Collapse Prevention (damage levels between 5 and 10).

  - For DSP(t_{tot}) greater than 20, the structure is vulnerable to exceeding performance level collapse prevention (damage levels between 10 and 15).
- Impulsivity Index (IP) of ground motion explicitly affects DSP(t_{tot}) robustness for detection of damage extent. So, the exact DSP(t_{tot}) that shows the extent of damage needs to consider the Impulsivity Index (IP) of ground motion.

References

[1] Rahami, H., Ghodrati Amiri, G., Amini Tehrani, H., & Akhavat, M. (2018). Structural Health Monitoring for Multi-story Shear Frames Based on Signal Processing Approach. Iranian Journal of Science and Technology, Transactions of Civil Engineering, 42(3), 287–303. https://doi.org/10.1007/s40996-018-0096-1.

[2] Kouchaki, M., Salkhordeh, M., Mashayekhi, M., Mirtaheri, M., & Amanollah, H. (2023). Damage detection in power transmission towers using machine learning algorithms. Structures, 56, 104980. https://doi.org/10.1016/j.istruc.2023.104980.

[3] Kaveh, A., Rahmani, P., & Dadras Eslamlou, A. (2021). Guided Water Strider Algorithm for Structural Damage Detection Using Incomplete Modal Data. Iranian Journal of Science and Technology, Transactions of Civil Engineering, 46(2), 771–788. https://doi.org/10.1007/s40996-020-00552-0.

[4] Avci, O., Abdeljaber, O., Kiranyaz, S., Hussein, M., Gabbouj, M., & Inman, D. J. (2021). A review of vibration-based damage detection in civil structures: From traditional methods to Machine Learning and Deep Learning applications. Mechanical Systems and Signal Processing, 147, 107077. https://doi.org/10.1016/j.ymssp.2020.107077.

[5] Qiao, L., & Esmaeily, A. (2011). An Overview of Signal-Based Damage Detection Methods. Applied Mechanics and Materials, 94–96, 834–851. https://doi.org/10.4028/www.scientific.net/amm.94-96.834.

[6] Rytter, A. (1993). Vibrational Based Inspection of Civil Engineering Structures. PhD Thesis, University of Aalborg, Aaloborg, Denmark.

[7] Carden, E. P., & Fanning, P. (2004). Vibration Based Condition Monitoring: A Review. Structural Health Monitoring, 3(4), 355–377. https://doi.org/10.1177/1475921704047500.

[8] Hou, R., & Xia, Y. (2021). Review on the new development of vibration-based damage identification for civil engineering structures: 2010–2019. Journal of Sound and Vibration, 491, 115741. https://doi.org/10.1016/j.jsv.2020.115741.

[9] Mallat, S. (1999). A wavelet tour of signal processing. Academic Press, Cambridge, United States.

[10] Rao, R. M. (1998). Wavelet transforms: Introduction to theory and applications. Pearson Education India, Noida, India.

[11] Amanollah, H., Asghari, A., Mashayekhi, M., & Zahrai, S. M. (2023). Damage detection of structures based on wavelet analysis using improved AlexNet. Structures, 56, 105019. https://doi.org/10.1016/j.istruc.2023.105019.

[12] Beheshti-Aval, S. B., Taherinasab, M., & Noori, M. (2013). Some precautions to consider in using wavelet transformation for damage detection analysis of plates. Smart Structures and Systems, 11(1), 35–51. https://doi.org/10.12989/sss.2013.11.1.03.

[13] Chakraverty, S., & Biswas, P. (2020). Recent Trends in Wave Mechanics and Vibrations. Springer Singapore. https://doi.org/10.1007/978-981-15-0287-3.

[14] Khatam, H., Golafshani, A. A., Beheshti-Aval, S. B., & Noori, M. (2007). Harmonic Class Loading for Damage Identification in Beams Using Wavelet Analysis. Structural Health Monitoring, 6(1), 67–80. https://doi.org/10.1177/1475921707072064.

[15] Newland, D. E. (1994). Wavelet Analysis of Vibration: Part 1—Theory. Journal of Vibration and Acoustics, 116(4), 409–416. https://doi.org/10.1115/1.2930443.

[16] Newland, D. E. (1994). Wavelet Analysis of Vibration: Part 2—Wavelet Maps. Journal of Vibration and Acoustics, 116(4), 417–425. https://doi.org/10.1115/1.2930444.

[17] Surace, C. & Ruotolo, R. (1994). Crack detection of a beam using the wavelet transform. Proceedings of the 12th International Modal Analysis Conference, 31 January-3 February, 1994, Honolulu, United States.

[18] Liew, K. M., & Wang, Q. (1998). Application of Wavelet Theory for Crack Identification in Structures. Journal of Engineering Mechanics, 124(2), 152–157. https://doi.org/10.1061/(asce)0733-9399(1998)124:2(152).

[19] Wang, Q., & Deng, X. (1999). Damage detection with spatial wavelets. International Journal of Solids and Structures, 36(23), 3443–3468. https://doi.org/10.1016/s0020-7683(98)00152-8.

[20] Bayissa, W. L., Haritos, N., & Thelandersson, S. (2008). Vibration-based structural damage identification using wavelet transform. Mechanical Systems and Signal Processing, 22(5), 1194–1215. https://doi.org/10.1016/j.ymssp.2007.11.001.

[21] Patel, S. S., Chourasia, A. P., Panigrahi, S. K., Parashar, J., Parvez, N., & Kumar, M. (2016). Damage Identification of RC Structures Using Wavelet Transformation. Procedia Engineering, 144, 336–342. https://doi.org/10.1016/j.proeng.2016.05.141.

[22] Jahangir, H., Hasani, H., & Esfahani, M. R. (2021). Wavelet-based damage localization and severity estimation of experimental RC beams subjected to gradual static bending tests. Structures, 34, 3055–3069. https://doi.org/10.1016/j.istruc.2021.09.059.

[23] Fallahian, M., Ahmadi, E., & Khoshnoudian, F. (2022). A structural damage detection algorithm based on discrete wavelet transform and ensemble pattern recognition models. Journal of Civil Structural Health Monitoring, 12(2), 323–338. https://doi.org/10.1007/s13349-021-00546-0.

[24] Thoriya, A., Vora, T., Jadeja, R., Ali Abdelrahman Ali, Y., & Patel, S. K. (2024). Application of wavelet transform techniques for corrosion assessment of embedded rebars in RC elements using electromechanical impedance. Measurement, 226, 114081. https://doi:10.1016/j.measurement.2023.114081.

[25] Beheshti-Aval, S. B., Taherinasab, M., & Noori, M. (2011). Using harmonic class loading for damage identification

of plates by wavelet transformation approach. Smart Structures and Systems, 8(3), 253–274. https://doi.org/10.12989/sss.2011.8.3.253.

[26] Mashayekhi, M., Estekanchi, H. E., Vafai, H., & Mirfarhadi, S. A. (2018). Development of hysteretic energy compatible endurance time excitations and its application. Engineering Structures, 177, 753–769. https://doi.org/10.1016/j.engstruct.2018.09.089.

[27] Sadeghi-Movahhed, A., Billah, A. H. M. M., Shirkhani, A., Mashayekhi, M., & Majdi, A. (2024). Vulnerability assessment of tall isolated steel building under variable earthquake hazard levels using endurance time method. Journal of Structural Integrity and Maintenance, 9(1). https://doi.org/10.1080/24705314.2024.2314816.

[28] Hou, Z., Noori, M., & Amand, R. St. (2000). Wavelet-Based Approach for Structural Damage Detection. Journal of Engineering Mechanics, 126(7), 677–683. https://doi.org/10.1061/(asce)0733-9399(2000)126:7(677).

[29] Goggins, J., Broderick, B. M., Basu, B., & Elghazouli, A. Y. (2007). Investigation of the seismic response of braced frames using wavelet analysis. Structural Control and Health Monitoring, 14(4), 627–648. https://doi.org/10.1002/stc.180.

[30] Todorovska, M. I., & Trifunac, M. D. (2010). Earthquake damage detection in the Imperial County Services Building II: Analysis of novelties via wavelets. Structural Control and Health Monitoring, 17(8), 895–917. https://doi.org/10.1002/stc.350.

[31] Vafaei, M., & Adnan, A. bin. (2012). Seismic damage detection of tall airport traffic control towers using wavelet analysis. Structure and Infrastructure Engineering, 10(1), 106–127. https://doi.org/10.1080/15732479.2012.704051.

[32] Aguirre, D. A., Gaviria, C. A., & Montejo, L. A. (2013). Wavelet-Based Damage Detection in Reinforced Concrete Structures Subjected to Seismic Excitations. Journal of Earthquake Engineering, 17(8), 1103–1125. https://doi.org/10.1080/13632469.2013.804467.

[33] Quiñones, M. M., Montejo, L. A., & Jang, S. (2015). Experimental and numerical evaluation of wavelet based damage detection methodologies. International Journal of Advanced Structural Engineering, 7(1), 69–80. https://doi.org/10.1007/s40091-015-0084-7.

[34] Pnevmatikos, N. G., & Hatzigeorgiou, G. D. (2016). Damage detection of framed structures subjected to earthquake excitation using discrete wavelet analysis. Bulletin of Earthquake Engineering, 15(1), 227–248. https://doi.org/10.1007/s10518-016-9962-z.

[35] He, H., Chen, Y., & Lan, B. (2021). Damage assessment for structure subjected to earthquake using wavelet packet decomposition and time-varying frequency. Structures, 34, 449–461. https://doi.org/10.1016/j.istruc.2021.07.087.

[36] FEMA 273. (1997). NEHRP Guidelines for the Seismic Rehabilitation of Buildings. Federal emergency Management Agency (FEMA), Building Seismic Safety Council, Washington, United States.

[37] Li, H., Yi, T., Gu, M., & Huo, L. (2009). Evaluation of earthquake-induced structural damages by wavelet transform. Progress in Natural Science, 19(4), 461–470. https://doi.org/10.1016/j.pnsc.2008.09.002.

[38] Hou, Z., Hera, A., & Shinde, A. (2006). Wavelet-Based Structural Health Monitoring of Earthquake Excited Structures. Computer-Aided Civil and Infrastructure Engineering, 21(4), 268–279. https://doi.org/10.1111/j.1467-8667.2006.00434.x.

[39] Aghajanzadeh, S. M., & Mashayekhi, M. (2024). Identifying earthquake-induced structural damage with normalized discrete wavelet coefficients. Asian Journal of Civil Engineering. https://doi.org/10.1007/s42107-024-01004-0.

[40] Kim, H., & Melhem, H. (2004). Damage detection of structures by wavelet analysis. Engineering Structures, 26(3), 347–362. https://doi.org/10.1016/j.engstruct.2003.10.008.

[41] Fajfar, P., & Krawinkler, H. (2022). Seismic design methodologies for the next generation of codes. Seismic Design Practice into the Next Century, 459–466, Routledge, Milton Park, United Kingdom. https://doi.org/10.1201/9780203740026-63.

[42] Pavel, F., & Lungu, D. (2013). Correlations Between Frequency Content Indicators of Strong Ground Motions and PGV. Journal of Earthquake Engineering, 17(4), 543–559. https://doi.org/10.1080/13632469.2012.762957.

[43] Panella, D. S., Tornello, M. E., & Frau, C. D. (2017). A simple and intuitive procedure to identify pulse-like ground motions. Soil Dynamics and Earthquake Engineering, 94, 234–243. https://doi.org/10.1016/j.soildyn.2017.01.020.